Acta Crystallographica Section D
Biological Crystallography
ISSN 0907-4449

Bound-solvent structures for microgravity-, ground control-, gel- and microbatch-grown hen egg-white lysozyme crystals at 1.8 Å resolution

Jun Dong,[a]† Titus J. Boggon,[a]‡ Naomi E. Chayen,[b] James Raftery,[a] Ru-Chang Bi[c] and John R. Helliwell[a]*

[a]Section of Structural Chemistry, Department of Chemistry, University of Manchester, M13 9PL, England, [b]Biophysics Section, Physics Department, Imperial College, London, SW7 2BZ, England, and [c]Institute of Biophysics, Academia Sinica, Beijing 100101, China

† Present address: Sir William Dunn School of Pathology, Oxford University, South Parks Road, Oxford OX1 3RE, England.
‡ Present address: Mount Sinai School of Medicine, 1425 Madison Avenue, New York, NY 10029, USA.

Correspondence e-mail: john.helliwell@man.ac.uk

Received 8 April 1998
Accepted 26 November 1998

PDB References: microgravity-grown lysozyme, 1bwj; ground-control-grown lysozyme, 1bwh; gel-grown lysozyme; microbatch-grown lysozyme, 1bwi.

A number of methods can be used to improve the stability of the protein crystal-growth environment, including growth in microgravity without an air–liquid phase boundary, growth in gels and growth under oil ('microbatch'). In this study, X-ray data has been collected from and structures refined for crystals of hen egg-white lysozyme (HEWL) grown using four different methods, liquid–liquid dialysis on Earth and in microgravity using the European Space Agency's (ESA) Advanced Protein Crystallization Facility (APCF) on board the NASA Space Shuttle Life and Microgravity Spacelab (LMS) mission (STS-78), crystallization in agarose gel using a tube liquid–gel diffusion method and crystallization in microbatch under oil. A comparison of the overall quality of the X-ray data, the protein structures and especially the bound-water structures has been carried out at 1.8 Å. The lysozyme protein structures corresponding to these four different crystallization methods remain similar. A small improvement in the bound-solvent structure is seen in lysozyme crystals grown in microgravity by liquid–liquid dialysis, which has a more stable fluid physics state in microgravity, and is consistent with a better formed protein crystal in microgravity.

1. Introduction

The driving rationale behind microgravity protein-crystal growth is that the reduction of buoyancy convection and sedimentation effects could improve the internal order of the growing crystal (see, for example, Helliwell, 1988). Hence, resolution limit and crystal mosaicity have been investigated in detail (Boggon *et al.*, 1998; Broutin *et al.*, 1997; Chayen *et al.*, 1996, 1997; Colapietro *et al.*, 1992; Fourme *et al.*, 1995; Helliwell *et al.*, 1996; Ng *et al.*, 1997; Riès-Kautt *et al.*, 1997; Smith *et al.*, 1996; Snell *et al.*, 1995; Snell, Casseta *et al.*, 1997; Snell, Boggon *et al.*, 1997; Strong *et al.*, 1992; Vaney *et al.*, 1996).

Since microgravity affects (stabilizes) fluid behaviour, it is surprising that the bound solvent has not been investigated. However, the effect on protein structure has been studied, *e.g.* for lysozyme (see Vaney *et al.*, 1996), and none found. This paper reports an analysis, especially of the bound solvent, including comparison with hen egg-white (HEWL) crystal structures for crystals grown as ground controls for the microgravity experiment, in agarose gel and in microbatch under paraffin oil.

Comparative studies of two microgravity-grown and one ground-grown lysozyme crystals (Dong, Wang *et al.*, 1998) showed that the ordered water molecules between protein molecules, which are bound by weak interactions, may have changed to some extent, involving in particular an increase in

the average numbers of hydrogen bonds per water molecule. More extensive studies and analyses have been undertaken and are presented here. This study also involves more accurate data, in particular the utilization of Mo $K\alpha$ to essentially eliminate absorption variations in the crystal which are well known to be able to adversely affect atomic displacement parameters. Moreover, we used the essentially identical X-ray beam intensity conditions of a home laboratory X-ray source, which facilitates data set intercomparisons.

The added significance of investigating the gel- and microbatch-grown crystal structures is twofold. The gel matrix may engender a similar benefit to that rendered by microgravity, *i.e.* in limiting solutal convection during the growth of protein crystals (Miller *et al.*, 1992). Microbatch crystallization under oil is a new technique which allows little or no contact with the container walls. We would like to investigate whether growth in this medium is also beneficial and whether paraffin oil has any effect on the protein structure and solvent binding in comparison with 'regular' crystal-growth methods.

2. Methods

2.1. Liquid–liquid dialysis in microgravity and on earth

Crystallization of the microgravity crystal studied here took place in the APCF onboard the NASA Space Shuttle's Life and Microgravity Spacelab (LMS) mission (STS-78). Identical material and reactors were used for both microgravity and ground control experiments. The APCF consists of 48 crystallization experiments of different geometries; vapour diffusion, free interface diffusion and liquid–liquid dialysis (Bosch *et al.*, 1992; Snyder *et al.*, 1991). The liquid–liquid dialysis geometry was used here. This reactor consists of three chambers; one containing protein and buffer solutions, one containing buffer and one containing salt solution. The salt solution is brought into contact with the protein and buffer by a 90° rotation of a plug which also contains salt solution. Crystal nucleation and growth occurs as the salt diffuses into the protein volume. The reactor is deactivated by a further 90° rotation of the plug. A solution of 21 mg of hen egg-white lysozyme (crystallized three times, dialyzed and lyophilized powder of chicken egg-white lysozyme supplied by Sigma, batch number L-6876 , lot 53H7145) dissolved in 250 µl 0.04 *M* acetate buffer (pH 4.7) was used to fill the protein chamber (188 µl). The salt chambers (541 µl) were filled with 1.35 *M* NaCl and the buffer chamber (59 µl) with 0.04 *M* acetate buffer (pH 4.7). Sodium azide was also added to the protein and buffer solution as an antifungal agent (1.92 mg per 188 µl). Crystallization took place at 293 ± 0.1 K for the microgravity case and at 293 ± 1 K for the ground control case, in which the reactor was held within a polystyrene box in a temperature-controlled room. The reactor was held in a vertical orientation with the protein chamber uppermost, *i.e.* the least turbulent orientation (Snell *et al.*, 1996). Crystals with typical dimensions ~0.5 × 0.5 × 0.6 mm initially nucleated after 25 h, with reactor deactivation occurring at the end of the mission (*i.e.* after 15 d).

2.2. Crystallization in gels

Protein crystallization using gels has been performed with a wide variety of protocols (Provost & Robert, 1991; García-Ruiz & Moreno, 1994). Here we have used a new method, the tube liquid–gel diffusion method (Dong, 1999), in order to obtain crystal growth with the least turbulence. HEWL crystals were grown in a gelled protein solution which consisted of 25 mg ml^{-1} lysozyme (Sigma, batch number L-6876, lot 53H7145), 0.2% agarose (Sigma, Type VII, of low gelling temperature), 4% NaCl (0.68 *M*), 4% MPD in acetate buffer (pH 4.5); the precipitating agent solution was 15% NaCl (2.57 *M*) and 15% MPD in buffer. The glass tube used was 6 cm tall with an inner diameter of 4 mm. Crystals of typical dimensions ~0.7 × 0.6 × 0.6 mm grew within 7 d at room temperature.

2.3. Crystallization by the microbatch method under oil

Crystallization by the microbatch method under oil as a general technique was initiated in order to save on the consumption of material. Samples are dispensed and incubated under oil which is used as an inert sealant to prevent evaporation of 1–2 µl drops consisting of a mixture of protein and crystallizing agents (Chayen *et al.*, 1990, 1992, 1994). The batch method is mechanically and technically the simplest to set up of all the crystallization methods.

In addition to preventing evaporation, the presence of oil also protects the samples from airborne contamination (which can cause excess unwanted nucleation). This enhances the cleanliness of the trials, thereby facilitating higher accuracy and reproducibility of the experiments (Chayen *et al.*, 1993). Furthermore, the crystals are buoyed by the viscous oil and hence have very little or no contact with the container walls (Chayen, 1996, 1997, 1998). This mimics to some extent the effect of microgravity, in that there is little or no contact with the container walls, although the presence of oil does not prevent convection. It is thus likely to improve the quality of the resulting crystals.

A solution containing 40 mg ml^{-1} of lysozyme (Sigma batch number L-6876, lot 65H7025, *i.e.* a different Sigma sample to the experiments described above) in 10 m*M* sodium citrate buffer pH 4.7 was mixed in an eppendorf tube with equal volumes of 12% (2.05 *M*) sodium chloride (BDH). The mixture was filtered through a 0.22 µm filter and 8 µl drops were manually dispensed under paraffin oil using a Gilson micropipette. Over 20 identical drops were set up and, within a week, single crystals typically measuring 0.5 × 0.4 × 0.3 mm were obtained in most of the drops. Crystallization took place at a temperature of 291–293 K.

2.4. Data collection and processing

X-ray data collection for the microgravity-, ground control-, gel- and microbatch-grown HEWL crystals used an RU-200 X-ray rotating-anode source and Rigaku IIc IP area detector. In each case, only one crystal mounted at room temperature in a quartz capillary was used for data collection. An Mo $K\alpha$ (λ = 0.71 Å wavelength) target was used for data collection of the

Table 1
Data-collection protocol.

	Microgravity	Ground control	Gel	Microbatch
Crystal dimensions (mm)	0.5 × 0.5 × 0.35	0.7 × 0.5 × 0.45	0.7 × 0.7 × 0.6	0.4 × 0.4 × 0.2
T_{max}/T_{min}†	1.015	1.025	1.104	1.222
Crystal volume (mm^3)	0.088	0.158	0.294	0.032
Collimator diameter (mm)	0.5	0.5	0.5	0.5
Illuminated crystal volume (mm^3)	0.088‡	Max. 0.158, min. 0.113§	Max. 0.175, min. 0.15	0.032
Oscillation range used per image (°)	0.75 + 0.5	0.75 + 0.5 + 1.5	0.75 + 0.5	0.75 + 0.5 + 4
Crystal-to-detector distance (mm)	250 + 300	250 + 300 + 450¶	87 + 116	80 + 116 + 168
Exposure time (min)	30 + 20	30 + 20 + 30	15 + 7	20 + 10 + 2
Total degrees collected	60 + 60	60 + 60 + 60	60 + 48	60 + 60 + 60
Target	Mo $K\alpha$	Mo $K\alpha$	Cu $K\alpha$	Cu $K\alpha$
Space group	$P4_32_12$	$P4_32_12$	$P4_32_12$	$P4_32_12$
Unit-cell dimensions (Å)				
a	79.25	79.27	79.20	79.23
b	79.25	79.27	79.20	79.23
c	38.02	37.96	38.04	37.94
All data				
Resolution (Å)	99–1.7	99–1.7	99–1.7	99–1.7
$\langle I\rangle/\langle\sigma\rangle$††	19.8 (2.0)	22.0 (2.0)	32.0 (3.3)	22.6 (6.6)
Total data	57479	72955	68445	73591
Number of unique data	11846	12309	12433	12081
Completeness (%)	85.5	88.8	89.6	87.2
R_{merge}‡‡	0.072	0.069	0.068	0.077

† Calculated ratios of maximum and minimum transmision of the primary X-ray beam in each case. At Mo $K\alpha$ $\mu \simeq 0.1$ mm^{-1} and at Cu $K\alpha$ $\mu \simeq 1$ mm^{-1}. Any absorption variations at Mo $K\alpha$ for the microgravity and ground control case are essentially completely eliminated as a source of systematic error. ‡ Inspection of the *SCALEPACK* image-to-image scale factors showed that essentially the full crystal volume was bathed throughout, *i.e.* the scales lay within a range of 0.88–1.17 (these indicate that the longest direction through the crystal of $(0.5^2 + 0.35^2)^{1/2} = 0.61$ mm may have taken the crystal slightly out of the X-ray beam for a part of the angular range; the relative *B* factors per image with respect to the first one lay in the range −2.4 to 1.9, which for these extremes would make a 2.1-fold change in intensities at 1.7 Å resolution. § Inspection of the *SCALEPACK* image-to-image scale factors show that the slow-pass (40 min per degree) data images included the situation where the longest dimension of the ground control crystal was parallel to the incident X-ray beam and so the full crystal volume was bathed for a part of the angular range covered; for these diffraction images (∼40° angle coverage) the diffraction image *B* factors relative to the first image lay within the range −2 to 1.5, which for these extremes would make a 1.8-fold change in intensities at 1.7 Å for these ground control diffraction images as the extreme case. ¶ Because of the larger volume of the ground-control crystal, compared with the microgravity-grown crystal, an additional very quick pass data set of images was collected *i.e.* exposure times of 30 min for 1.5° rotation (equivalent to 10 min for 0.5° rotation so as to capture saturated spots at low resolution. †† For $\langle I\rangle/\langle\sigma\rangle$ the figure in parentheses is the value in the outer resolution shell. ‡‡ $R_{merge} = \sum|I_i - \langle I\rangle|/\sum I_i$, where I_i is the measured intensity of individual reflections and $\langle I\rangle$ the mean intensity of the symmetry-related measurements of this reflection.

microgravity and ground-control data sets and a Cu $K\alpha$ (λ = 1.54 Å wavelength) target was used for the gel- and microbatch-grown crystals. Ideally, Mo $K\alpha$ radiation should also have been used for these last two cases, but unfortunately this was not possible. However, the Cu $K\alpha$ to Mo $K\alpha$ comparisons are nevertheless also of interest. The exposure times for the gel- and microbatch-grown image frames were reduced for the longer wavelength copper-anode source to compensate for the enhanced crystal sample scattering efficiency at Cu $K\alpha$. The X-ray generator settings were 50 kV and 120 mA for each case. A summary of the data-collection protocols and processing results are given in Table 1. In using a rather divergent conventional X-ray source beam (∼ 0.5°) in these evaluations, we are obviously not harnessing the benefit that would accrue from any differences in crystal mosaicity with a non-divergent specially collimated synchrotron radiation beam and optimizable, for example, with a synchrotron radiation X-ray undulator (see Figs. 3 and 4 of Snell *et al.*, 1995). The data were processed using *DENZO* and scaled and merged using *SCALEPACK* (Otwinowski, 1993). The resulting R_{merge} and completeness of each of the four data sets, in resolution shells, are shown in Table 2; consideration of Table 2 and the point at which the merging *R* factors rise above 20% led to data for the model refinement being cut at 1.8 Å. Note that the illuminated volume of the microgravity crystal is about 0.7 times that of the ground control crystal and 0.6 times that of the gel-grown crystal. No adjustment of exposure time was made to take account of these differences. In effect this slightly 'disfavoured' the microgravity crystal compared with the two other crystals.

2.5. Model refinement

The starting model for refinement in each case was taken from the refined atomic coordinates (entry 193L) of HEWL obtained from the PDB (Vaney *et al.*, 1996), *i.e.* the best resolution structure of lysozyme yet refined (1.33 Å). All water molecules were removed from this initial model.

Data from 20 to 1.8 Å were used without any σ cutoff and 5% of the reflections were separated for use as a free *R* test (Brünger, 1992*a*). This model was then refined using *X-PLOR* (Brünger, 1992*b*), first with rigid-body refinement, followed by simulated-annealing and atomic displacement parameter (ADP) refinement and a number of rounds of positional and ADP refinement and model rebuilding in *O* (Jones & Kjeldgaard, 1993, 1994). A solvent mask was incorporated during refinement, with a solvent density of 0.34 e$^-$ Å^{-3} and a solvent radius of 0.25 Å used. The *PEAKMAX* and *WATPEAK* programs from the *CCP*4 program suite (Collaborative Computational Project, Number 4, 1994) were used to locate the water molecules at various stages of the refinement. Water molecules were inserted in the models with an initial isotropic *B* factor of 30 Å^2 if they formed at least one stereochemically reasonable hydrogen bond (between 2.5 and 3.4 Å) and were

Table 2
R_{merge} and completeness of the X-ray data sets collected from HEWL crystals grown in microgravity, as well as ground-control-, gel- and microbatch-grown cases.

Resolution (Å)	Microgravity		Ground control		Gel		Microbatch	
	R_{merge}†	Completeness (%)	R_{merge}†	Completeness (%)	R_{merge}†	Completeness (%)	R_{merge}†	Completeness (%)
99.00–4.19	0.054	95.1	0.056	98.8	0.050	98.3	0.054	96.6
4.19–3.33	0.064	98.8	0.064	99.2	0.063	99.9	0.074	98.8
3.33–2.91	0.075	99.2	0.070	97.1	0.073	99.9	0.090	98.2
2.91–2.64	0.085	99.6	0.080	97.5	0.080	100.0	0.096	96.7
2.64–2.45	0.093	99.9	0.090	96.6	0.086	100.0	0.107	97.0
2.45–2.31	0.093	99.6	0.090	97.7	0.091	100.0	0.113	96.6
2.31–2.19	0.099	99.3	0.097	96.9	0.090	95.6	0.113	95.1
2.19–2.10	0.105	98.1	0.105	96.1	0.081	91.9	0.112	91.8
2.10–2.02	0.120	94.3	0.116	94.9	0.090	91.8	0.110	92.7
2.02–1.95	0.135	88.8	0.139	92.1	0.107	91.0	0.116	92.0
1.95–1.89	0.165	77.3	0.163	88.7	0.126	89.3	0.122	92.8
1.89–1.83	0.186	66.5	0.187	81.4	0.152	87.2	0.124	89.0
1.83–1.78	0.239	62.1	0.249	70.9	0.172	76.5	0.127	70.3
1.78–1.74	0.271	54.5	0.255	64.3	0.191	68.0	0.136	53.9
1.74–1.70	0.393	45.1	0.344	56.1	0.232	51.8	0.151	43.2
Overall	0.072	85.5	0.069	88.8	0.068	89.6	0.077	87.2

† $R_{merge} = \sum |I_i - \langle I \rangle| / \sum I_i$, where I_i is the measured intensity of individual reflections and $\langle I \rangle$ the mean intensity of the symmetry-related measurements of this reflection.

above the 3 r.m.s. level in $F_o - F_c$ difference-density maps. If the electron density around a water at the end of any given round of refinement was less than one r.m.s. level in the $2F_o - F_c$ map then that water was deleted. Final model refinement statistics are given in Table 3.

3. Results and discussion

3.1. Comparison of the diffraction data

The intensities of the gel-grown crystal data set are improved significantly both at low resolution and high resolution compared with the microgravity-, ground control- and microbatch-grown crystal data (Fig. 1). This arises partly from the larger illuminated crystal volume, which is a factor of two greater than the microgravity-grown crystal and a factor of five greater than the microbatch-grown crystal values.

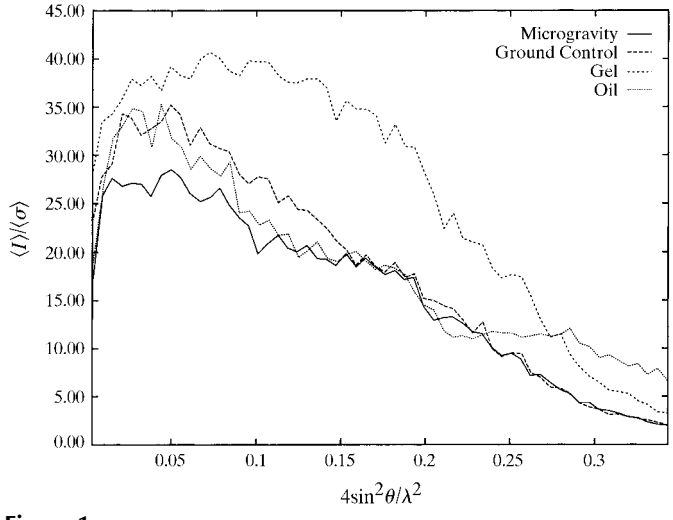

Figure 1
Average values of $\langle I \rangle / \langle \sigma \rangle$ plotted against $4\sin^2\theta/\lambda^2$ for the microgravity-, ground-control-, gel- and microbatch-grown crystals.

Although the illuminated crystal volume of the microgravity crystal is between 0.6 and 0.8 times that of the ground control crystal, the $\langle I \rangle / \langle \sigma \rangle$ values are essentially identical at medium to high resolution (R_{merge} values in Table 2; Fig. 1). In another study, Strong *et al.* (1992) noted a reduction in background residuals in microgravity-grown lysozyme crystals. Ahari *et al.* (1997), for a small-molecule crystal, noted considerably reduced disorder diffuse X-ray scattering for their microgravity-grown crystal; this would not only improve (*i.e.* reduce) the $\sigma(I)$s but also enhance the Bragg reflection intensities, both of which would improve $\langle I \rangle / \langle \sigma \rangle$.

The use of the different wavelengths (Mo $K\alpha$ and Cu $K\alpha$) appears to favour the Cu $K\alpha$ data sets, in that the gel-grown case is the best and the rather small microbatch-grown crystal still has similar R_{merge} (Table 1) and $\langle I \rangle / \langle \sigma \rangle$ trends (Fig. 1).

3.2. Cation- (Na^+) and anion- (Cl^-) binding sites

One cation-binding and one anion-binding site have been identified in tetragonal HEWL; Dong *et al.* (1995) ascribed the cation to be a calcium ion and Vaney *et al.* (1996) assigned it to be a sodium ion. Bentley *et al.* (1993), in a study of Japanese quail egg-white lysozyme, also found a sodium ion in the cation-binding site. The position of the cation-binding site shows electron density in all the four structures presented here. However, in the microgravity, ground control and gel structures, the density has been identified as a water based on its higher B factor and longer distances to surrounding atoms. In the microbatch-grown crystal structure, the side chain Ser72 has moved closer to the density peak of the cation-binding site than in the other three structures, and, therefore, no water molecule has been positioned there. Hence, the local protein structure around the position of the cation-binding site and the site itself are not conserved, whereas the Chinese and French HEWL structures (Dong *et al.*, 1995; Dong, Wang *et al.*, 1998; Vaney *et al.*, 1996) show stronger cation binding at that position. The most likely explanation of this is that HEWL

Table 3
Final model-refinement statistics for the microgravity-, ground-control-, gel- and microbatch-grown lysozyme structures.

The Protein Data Bank codes for the four structures are 1bwj, 1bwh, 1bvx and 1bwi, respectively.

	Microgravity	Ground control	Gel	Microbatch
Resolution limits (Å)	2.0–1.8	2.0–1.8	2.0–1.8	2.0–1.8
R_{free} factor (%)†	21.2 (23.1)	23.3 (25.6)	21.7 (30.2)	20.6 (32.9)
R factor (%)†‡	17.3 (27.7)	18.4 (27.5)	18.2 (30.7)	17.1 (25.9)
Number of reflections used ($F > 0$)	10735	10967	11073	10979
Number of protein atoms	1001	1001	1001	1001
Number of solvent molecules	104§	92‡	95‡	92‡
R.m.s. deviations from ideality				
Bond lengths (Å)	0.009	0.007	0.008	0.007
Bond angles (°)	1.904	1.566	1.616	1.579
Improper angles (°)	1.248	1.082	1.210	1.216
Dihedral angles (°)	22.34	21.92	22.19	22.20
Ramachandran plot details				
Number of residues in favoured regions	100	101	99	97
Number of residues in allowed regions	13	12	14	16
Number of residues in disallowed regions	0	0	0	0
Mean B factors (Å^2)				
Cα atoms	18.8	19.1	18.0	18.9
Main-chain protein atoms	19.0	19.4	18.0	19.1
Side-chain protein atoms	23.7	24.5	22.8	24.4
Over all protein atoms	21.3	21.9	20.3	21.7
Over all waters	36.7	37.6	36.8	37.1
Over whole structure	22.7	23.2	21.8	22.9
Number of hydrogen bonds				
Solvent to protein only	150	140	152	142
Solvent to all	241	221	225	231

† For R_{free} and R, the factors in parentheses are for the outer shell 1.88–1.8 Å. ‡ R factor = $\sum |F_o - F_c| / \sum |F_o|$. § Two of these water positions correspond to Na^+ and Cl^- ion binding sites (discussed in §3.2).

Table 4
Statistics of the water-molecule positions in the cation-binding site, as identified by Dong *et al.* (1995) and Vaney *et al.* (1996), compared with the statistics published by Dong, Wang *et al.* (1998).

	Microgravity	Ground control	Gel	Dong
Water label	140	173	176	Sodium
B factor (Å^2)	39.2	36.2	44.3	9.1
Bond length (Å)				
to O60	2.63	2.79	2.95	2.40
to O64	2.68	2.58	2.70	2.37
to OG72	2.66	2.68	2.63	2.52
to O73	2.48	2.90	2.79	2.55
to OH2	Wat142, 3.22	Wat172, 2.95	Wat155, 2.98	Wat174, 2.53; Wat188, 2.57

obtained from different sources can have different sodium contents, so a strongly bound sodium ion occurs in crystals from lysozyme samples with a high sodium content. This has been investigated by atomic absorption spectroscopy demonstrating that the strongly bound sodium lysozyme sample has a high sodium ion content (Dong, Wang *et al.*, 1998). There is then no sodium ion binding site in our HEWL samples, which must have lower sodium content than those presented in Vaney *et al.* (1996) and Dong, Wang *et al.* (1998). It is also of note that when a strongly bound cation is found, the local protein structure (part of a loop region) moves towards the cation compared with the weaker binding water case (Table 4). A comparison of the three waters modelled at this site to the strongly bonded cation identified by Dong *et al.* (1995) is shown in Table 4.

In contrast, the chloride ion binding site is highly conserved in all four structures studied here.

3.3. Protein structure comparisons

The lysozyme protein structures from the 1.8 Å model refinements were compared. All four structures are high-quality structures as evidenced from *PROCHECK* (Laskowski *et al.*, 1993), *e.g.* in terms of placement of residues of favoured and allowed regions of the Ramachandran plot (Table 3). There are very subtle changes involving two or fewer residues moving between allowed and favoured regions and *vice versa*. The model geometry residuals (Table 3) are also very good. A structural change at Ser72 in the microbatch case has been noted in §3.2. The r.m.s. overlap of Cα, main-chain and all protein atoms of each structure (excluding residues 72 and 73) using *LSQKAB* (Kabsch, 1976) yields the values in Table 5, all of which show close agreement. These protein structures are very similiar.

3.4. Bound-solvent structure comparisons

The ordered water molecules were analysed for the four HEWL crystal structures. In the microgravity-, ground control-, gel- and microbatch-grown lysozyme crystals 104, 92, 95 and 92 water molecules, respectively, were identified in the asymmetric unit. The microgravity-grown structure has a greater number of waters than the gel-grown structure, and the gel-grown structure has a greater number of waters than the ground control- and microbatch-grown crystal structures. The distances of the water molecules from the nearest protein atom define the primary and secondary solvent shells, whereby waters closer than 3.4 Å to the protein are considered to be in the primary hydration shell and those further away in the secondary hydration shell. The microgravity case has an increase in the numbers of both primary and secondary waters compared with the other three structures (Fig. 2). Overall, the gel-grown structure has a few more waters than the ground control- and microbatch-grown structures. More ordered waters are identified in the primary hydration shell than the secondary hydration shell, which is as expected.

3.4.1. Bound-water *B*-factor analysis. There were 59 common waters conserved between the four structures. These

Table 5
The results of r.m.s. overlap numbers fitted (in Å^2) by Cα, main-chain and all protein atoms (excluding residues 72 and 73) between each protein structure.

	Cα	Main chain	All protein atoms
Microgravity–ground control	0.083	0.121	0.301
Microgravity–gel	0.101	0.150	0.363
Microgravity–oil	0.108	0.112	0.324
Ground control–gel	0.095	0.132	0.261
Ground control–oil	0.107	0.129	0.288
Gel–oil	0.101	0.158	0.321

waters were principally in the primary hydration shell, with average B factors of 29.8, 31.3, 30.7 and 32.3 Å^2 in the microgravity-, ground-control-, gel- and microbatch-grown cases, respectively. A water was considered common if there was a distance of less than 1.0 Å between it and a water from another structure, as determined using the program *DISTANG* (IUPAC–IUB Conventions, 1972) from the *CCP*4 program suite (Collaborative Computational Project, Number 4, 1994). The microgravity case gives a percentage increase in intensity of these 59 conserved waters of 26, 15 and 47% at 1.8 Å owing to the lower B factors compared to the ground control, gel and microbatch cases, respectively, using equation (1), where ΔB is the difference in B factor, θ is the angle of maximum diffraction, λ is the wavelength of X-rays and ΔI is their change in intensity.

$$\Delta I = \exp\left(\frac{2\Delta B \sin^2\theta}{\lambda^2}\right). \quad (1)$$

A mean B-factor analysis of the common waters between six pairings of the four structures was carried out. The microgravity case showed a B-factor improvement of 1.3 Å^2 over the ground control waters found in common positions. Using equation (1) this corresponds to a 22% improvement in data intensity at 1.8 Å resolution from these waters (Table 6), *i.e.* since the bound waters are ∼10% of the ordered atoms in the crystal this would yield an overall intensity increase from the crystal of 2.2% at the edge of the pattern (1.8 Å). Table 6 summarizes the common water pairing, the B factors of each water population and the improvement in their diffracted intensities owing to changes in B factor at the outer edge (1.8 Å) of the diffraction pattern.

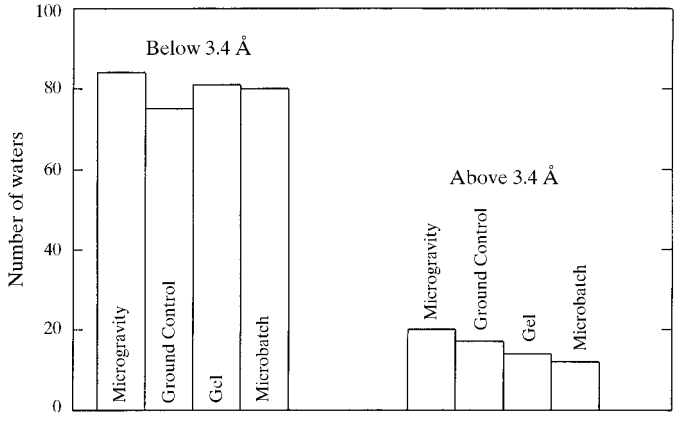

Figure 2
Histogram showing the numbers of bound waters in the primary and secondary hydration shells (distance from water to the nearest protein atom less than and greater than 3.4 Å, respectively).

The B factors for the protein atoms have values 21.3, 21.9, 20.3 and 21.7 Å^2 for the microgravity-, ground control-, gel- and microbatch-grown structures, respectively. Between the microgravity and ground control structures, both of which were refined against Mo $K\alpha$ short-wavelength data, the difference in B factors of 0.6 compares with a ΔB for the common waters of 1.3 (Table 6). Combined with the increase in the number of bound waters for the microgravity, these are small but nevertheless consistent changes over the ground control. The largest difference between protein atom B values are those for the ground control (21.9) and the gel (20.3) cases, *i.e.* a ΔB of 1.6. For this pair, the common waters show a ΔB of 0.6. The ΔB of 0.6 is very small, although in the correct sense considering there are more bound waters in the gel case. The use of Cu $K\alpha$ for the gel data must mean that the gel/ground-control comparison will be more vulnerable to errors than the microgravity/ground-control cases studied with the same short X-ray wavelength. Nevertheless, the gel case looks favourable compared with the ground control case, although inferior to the microgravity case (in terms of bound waters). The sensitivity of these B values and the small ΔB values to the refinement software warranted further checks, although the use of *X-PLOR* here for the model refinement for the four cases was the same as described in §2.5. The *CCP*4 protein model-refinement program *REFMAC* has been used for the ground-control and microgravity cases in order to assess sensitivity. The small difference in B factors is still seen (1.3 in favour of the microgravity-grown structure, *i.e.* $\langle B \rangle$ for the microgravity case common waters of 32.2 compared with 33.5 for the ground-control case) now with 70 common waters between the structures rather than 69. In a final refinement check, using the common 10115 reflections and *REFMAC*, these values were 32.1 for the microgravity case and 33.4 for the ground-control case, again then with a ΔB of 1.3 in favour of the microgravity-grown structure.

3.4.2. Total sum of hydrogen bonds involving the bound waters. Ordered water molecules are connected with the protein atoms or other water molecules by hydrogen bonds. A sum of the total number of hydrogen bonds formed by the water molecules was 241, 221, 225 and 231, respectively, for the microgravity-, ground control-, gel- and microbatch-grown crystal structures. More hydrogen bonds lead to a more stable structure and a higher quality protein crystal. This, then, is evidence at the atomic level that microgravity can improve the quality of protein crystals *via* an improved bound-solvent structure. However, since water molecules exchange rapidly with the solvent, it is puzzling that a more ordered bound-solvent structure should be preserved on the return to earth of a microgravity-grown crystal. Most likely, then, is that in the microgravity-grown crystal the weaker intermolecular interactions, *i.e.* involving bound solvent, are more clearly resolved. Once 'better formed' in space, the crystal remains 'better formed' on its return to earth.

Table 6
B-factor analysis of common waters between the four structures showing the improvement in their diffracted intensity from the common waters at 1.8 Å.

Improvement in intensity is calculated using equation (1). Mg, microgravity; GC, ground control; Oil, microbatch.

First pair	Second pair	Number of common waters	First mean *B* factor	Second mean *B* factor	Difference in *B* factors	ΔI (%)
Oil	GC	73	34.3	34.2	0.1	2
GC	Gel	73	34.2	33.6	0.6	10
Oil	Gel	71	34.0	33.0	1.0	17
GC	Mg	69	33.0	31.7	1.3	22
Gel	Mg	72	33.5	32.0	1.5	26
Oil	Mg	71	34.4	32.1	2.3	43

4. Concluding remarks

The use of Mo $K\alpha$ radiation of very short wavelength essentially eliminated crystal sample absorption as a source of experimental error between the microgravity and ground-control data sets. A comparison of the four HEWL crystal structures has shown that, at this resolution, the protein structures remain very similar. One difference was noted in that the Na^+ ion site was not conserved in the microbatch structure, but overall there is no significant impact on the protein structure for the crystal grown under paraffin oil. However, the ordered water molecules, which are bound by weak interactions, alter between the structures, with the microgravity case indicating a better ordered bound solvent (for the common waters) and having an increased number of bound waters, and the gel-grown case approaching this. These results are in accordance with the expected stabilities of the fluid in liquid–liquid geometry in microgravity, as used here [*i.e.* vapour-diffusion droplet geometry, and the possibility of Marangoni convection have both been avoided (Chayen *et al.* (1997)], compared with situations of convective flow of liquids and/or sedimentation of nuclei or crystals on earth. A better formed protein crystal has resulted where the weaker intermolecular interactions, *i.e.* involving bound solvent, are more clearly resolved. It is interesting that the microgravity crystal used was smaller than the earth-grown ground-control crystal and yet had very similar $\langle I\rangle/\langle\sigma\rangle$ distributions at medium to high resolution; this is consistent with the results of Strong *et al.* (1992) (also on lysozyme) and of Ahari *et al.* (1997) (for a small-molecule crystal in microgravity *versus* ground comparison). Our results show that the bound-solvent structure, which comprises ~10% of the ordered atoms, can be improved *via* microgravity protein crystal growth, although the changes are small. Protein crystals with higher solvent contents may be a particular category of protein crystal that might benefit more from the microgravity environment (Dong, Pan *et al.*, 1998) and also crystals where there are rather few lattice intermolecular interactions, thus making the whole crystal better formed.

Drs J. Stapelmann, R. Bosch, P. Lautenschlager and L. Potthast of Dornier GmbH as well as Drs H. U. Walter, K. Fuhrmann and O. Minster at ESA are thanked for their continuing help and support with the APCF. The Wellcome Trust funded the Manchester R-AXIS, SERC (now EPSRC) funded the rotating-anode X-ray generator and BBSRC funded the Silicon Graphics computer workstations and molecular graphics, to whom JRH is very grateful. JRH also thanks BBSRC for 33% salary support of JR. NC thanks BBSRC for support. TJB thanks the University of Manchester and the Samuel Hall fund for PhD studentship support. JD was supported by the Royal Society for a one year Queen Elizabeth II Fellowship with JRH in Manchester, on leave from Beijing. NC and JRH acknowledge the support of the EU Protein Crystallogenesis Network.

References

Ahari, H., Bedard, R. L., Bowes, C. L., Coombs, N., Dag, Ö., Jiang, T., Ozin, G. A., Petrov, S., Sokolov, I., Verma, A., Vovk, G. & Young, D. (1997). *Nature (London)*, **388**, 857–860.
Bentley, G. (1993). Protein Data Bank entry 2IHL.
Boggon, T. J., Chayen, N. E., Dong, J., Lautenschlager, P., Potthast, L., Siddons, P., Stojanoff, V., Gordon, E., Thompson, A., Snell, E. H., Bi, R. C., Zagalsky, P. F. & Helliwell, J. R. (1998). *Philos. Trans. R. Soc. London*, **356**, 1045–1061.
Bosch, R., Lautenschlager, P., Potthast, L. & Stapelmann, J. (1992). *J. Cryst. Growth*, **122**, 310–316.
Broutin, I., Riès-Kautt, M. & Ducruix, A. (1997). *J. Cryst. Growth*, **181**, 97–108.
Brünger, A. T. (1992*a*). *X-PLOR Manual, version* 3.1. *A System for X-ray Crystallography and NMR*. New Haven & London: Yale University Press.
Brünger, A. T. (1992*b*). *Nature (London)*, **355**, 472–475.
Chayen, N. E. (1996). *Protein Eng.* **9**(10), 927–929.
Chayen, N. E. (1997). *Structure*, **5**, 1269–1274.
Chayen, N. E. (1998). *Acta Cryst.* D**54**, 8–15.
Chayen, N. E, Boggon, T. J., Cassetta, A., Deacon, A., Gleichmann, T., Habash, J., Harrop, S. J., Helliwell, J. R., Nieh, Y. P., Peterson, M. R., Raftery, J., Snell, E. H., Hädener, A., Niemann, A. C., Siddons, D. P., Stojanoff, V., Thompson, A. W., Ursby, T. & Wulff, M. (1996). *Quart. Rev. Biophys.* **29**, 227–278.
Chayen, N. E., Radcliffe, J. W. & Blow, D.M. (1993). *Protein Sci.* **2**, 113–118.
Chayen, N. E., Shaw Stewart, P. D. & Baldock, P. (1994). *Acta Cryst.* D**50**, 456–458.
Chayen, N. E., Shaw Stewart, P. D. & Blow, D. M. (1992). *J. Cryst. Growth*, **122**, 176–180.
Chayen, N. E., Shaw Stewart, P. D., Maeder, D. & Blow, D. M. (1990). *J. Appl. Cryst.* **23**, 297–302.
Chayen, N. E., Snell, E. H., Helliwell, J. R. & Zagalsky, P. F. (1997). *J. Cryst. Growth*, **171**, 219–225.
Colapietro, M., Cappuccio, G., Marciante, C., Pifferi, A., Spagna, R. & Helliwell, J. R. (1992). *J. Appl. Cryst.* **25**, 192–194.
Collaborative Computational Project, Number 4 (1994). *Acta Cryst.* D**50**, 760–763.
Dong, J. (1999). In preparation.
Dong, J., Han, Q., Chu, N. M. & Bi, R. C. (1995). *Chin. Sci. Bull.* **40**(8), 672–677.
Dong, J., Pan, J., Wang, Y. & Bi, R. C. (1998). *Space Med. Med. Eng.* **11**(1), 26–29.

Dong, J., Wang, Y. P., Han, Q. & Bi, R. C. (1998). *Sci. Chin*, **41**(3), 238–244.
Fourme, R., Ducruix, A., Riès-Kautt, M. & Capelle, B. (1995). *J. Synchrotron Rad.* **2**, 136–142.
García-Ruiz, J. M. & Moreno, A. (1994). *Acta Cryst.* D**50**, 484–490.
Helliwell, J. R. (1988). *J. Cryst. Growth*, **90**, 259–272.
Helliwell, J. R, Snell, E. H. & Weisgerber, S. (1996). *Proceedings of 1995 Berlin Microgravity Conference*, edited by L. Ratke, H. Walter & B. Feuerbacher, pp. 155–170. Berlin/Heidelberg: Springer-Verlag.
IUPAC–IUB Conventions (1972). *J. Mol. Biol.* **50**, 1.
Jones, T. A. & Kjeldgaard, M. (1993). *O Manual, version* 9. Uppsala University, Sweden.
Jones, T. A. & Kjeldgaard, M. (1994). *Proceedings of the CCP4 Study Weekend. From First Map to Final Model*, edited by S. Bailey, R. Hubbard & D. Waller, pp. 1–13. Warrington: Daresbury Laboratory.
Kabsch, W. (1976). *Acta Cryst.* A**32**, 922–923.
Laskowski, R. A., MacArthur, M. W., Moss, D. S. & Thornton, J. M. (1993). *J. Appl. Cryst.* **26**, 283–291.
Miller, T. Y., He, X. & Carter, D. C. (1992). *J. Cryst. Growth*, **122**, 306–309.
Ng, J., Lorber, B., Giegé, R., Koszelak, S., Day, J., Greenwood, A. & McPherson, A. (1997). *Acta Cryst.* D**53**, 724–733.
Otwinowski, Z. (1993). *Proceedings of the CCP4 Study Weekend. Data Collection and Processing*, edited by L. Sawyer, N. Isaacs & S. Bailey, pp. 56–62. Warrington: Daresbury Laboratory.
Provost, K. & Robert, M. C. (1991). *J. Cryst. Growth*, **110**, 258–264.
Riès-Kautt, M., Broutin, I., Ducruix, A., Shepard, W., Kahn, R., Chayen, N. E., Blow, D., Paal, K., Littke, W., Lorber, B., Théobald-Dietrich, A. & Giegé, R. (1997). *J. Cryst. Growth*, **181**, 79–96.
Smith, G. D., Ciszak, E. & Pangborn, W. A. (1996). *Protein Sci.* **5**, 1502–1511.
Snell, E. H., Boggon, T. J., Helliwell, J. R., Moskowitz, M. E. & Nadarajah, A. (1997). *Acta Cryst.* D**53**, 747–755.
Snell, E. H, Cassetta, A., Helliwell, J. R., Boggon, T. J., Chayen, N. E., Weckert, E., Hölzer, K., Schroer, K., Gordon, E. J. & Zagalsky, P. F. (1997). *Acta Cryst.* D**53**, 231–239.
Snell, E. H., Helliwell, J. R., Boggon, T. J., Lautenschlager, P. & Potthast, L. (1996). *Acta Cryst.* D**52**, 529–533.
Snell, E. H, Weisgerber, S., Helliwell, J. R., Weckert, E., Hölzer, K. & Schroer, K. (1995). *Acta Cryst.* D**51**, 1099–1102.
Snyder, R. S, Fuhrmann, K. & Walter, H. U. (1991). *J. Cryst. Growth*, **110**, 333–338.
Strong, R. K., Stoddard, B. L., Arrott, A. & Farber, G. K. (1992). *J. Cryst. Growth*, **119**, 200–214.
Vaney, M. C., Maignan, S., Riès-Kautt, M. & Ducruix, A. (1996). *Acta Cryst.* D**52**, 505–517.